Supplement of Atmos. Chem. Phys., 26, 5123–5150, 2026
https://doi.org/10.5194/acp-26-5123-2026-supplement

Atmospheric Chemistry and Physics
Open Access
EGU

Supplement of

Revisiting the global budget of atmospheric glyoxal: updates on terrestrial and marine precursor emissions, chemistry, and impacts on atmospheric oxidation capacity

Aoxing Zhang et al.

Correspondence to: Tzung-May Fu (fuzm@sustech.edu.cn) and Yuhang Wang (yuhang.wang@eas.gatech.edu)

S1. Calculation of glyoxal yields using DSMACC

Our DSMACC simulations were set to the meteorological and chemical environments of a surface location in Southern China (Zou et al., 2023). The meteorological and chemical variables were fixed based on measurements from a field campaign in Hong Kong SAR, China (Xiong et al., 2025): atmospheric surface pressure 1007 hPa; surface temperature 293 K; 5×10^3 ppm of H_2O (relative humidity of 22%), 0.7 ppm of CO, 40 ppb of O_3.

To constrain the production and concentration of OH in the model, two proxy compounds (named OHPRE and OHDECAY) were added in the mechanisms as a producer and consumer of OH. Under a typical NO_x concentration (1 ppb), we constrained a baseline OHPRE and OHDECAY to get a daily mean OH production rate of 1.3×10^6 molecules cm^{-3} s^{-1} with daily mean OH concentration of 1.6×10^6 molecules cm^{-3}. We conducted sensitivity simulations with NO concentrations ranging from 0.1 ppb to 5 ppb, assuming an ambient NO_2-to-NO concentration ratio of 4. At each NO_x sensitivity experiment, we perturb OHPRE and OHDECAY by scale factors from 0.01 to 100, in order to cover realistic conditions of NO_x and OH concentrations in the atmosphere.

To quantify the glyoxal yields from different mechanisms, we constructed three distinct DSMACC models: D-MCM, D-GC, and D-GCnew. The D-MCM model incorporated the photochemical degradation of isoprene from MCM v3.3.1, which includes 611 intermediate species and 1944 chemical reactions, representing the most comprehensive representation of isoprene chemistry currently available. The D-GC and D-GCnew models adopted the default isoprene chemical mechanisms from GEOS-Chem version 14.2.3 and the updated mechanisms developed in this study, respectively. DSMACC used the Kinetic Pre-Processor (KPP) (Sandu and Sander, 2006; Lin et al., 2023) to process kinetics chemical mechanisms. KPP used an implicit solver to deal with fast chemical reactions with radicals, making the chemical state in DSMACC sensitive to the radical production rate. Because not all radicals sources were included in DSMACC experiments, the radical production rates were different from the real condition and were more sensitive to NO_x concentrations. Therefore, rather than constraining HO_x concentrations, we created a dummy OH source in DSMACC to produce OH radicals at a constant rate (1.3×10^6 molec cm^{-3} s^{-1})

To quantify glyoxal yields from isoprene, we initialized the model with 1 ppb isoprene for all experiments. We turned off the chemical reactions removing glyoxal in all DSMACC experiments, and the simulation period was 96 hours, much larger than the lifetime of isoprene. Then the ratio of the final glyoxal concentration and the precursor's initial concentration is the glyoxal yield derived from DSMACC.

Table S1. Observed surface or boundary layer mean glyoxal concentration over land and ocean. Surface glyoxal concentrations are reported unless otherwise noted.

Name	Latitude	Longitude	Period	Hour of Day	Glyoxal (ppt)	Reference
Ocean						
Salt Point	39°N	123°W	Aug–Sep 2005	11–14 Local time	20	Seaman et al. (2006)
Caribbean Sea	15°N	66°W	Oct 1988	Daily mean	40	Zhou and Mopper (1990)
Sargasso Sea coast	15°N–27°N	94°W–66°W	Oct 1988–Mar 1989	Daily mean	80	Zhou and Mopper (1990)
Tropical Pacific NH	5°N–20°N	133°W–110°W	Jan–Mar 2012	Daily mean	32	Coburn et al. (2014)
Tropical Pacific SH	5°S–10°S	110°W–93°W	Jan–Mar 2012	Daily mean	43	Coburn et al. (2014)
TP NH aircraft RF12	8.5°N	101.5°W	Jan–Feb 2012	Daily mean	25	Volkamer et al. (2015), 0–2 km mean
TP NH aircraft RF17	6°N–7°N	90°W–92°W	Jan–Feb 2012	Daily mean	34	Volkamer et al. (2015), 0–2 km mean
Cape Grim	40°S–44°S	140°E–144°E	Aug–Sep 2011	Daily mean	7	Lawson et al. (2015)
Chatham Rise	40°S–50°S	175°E–175°W	Feb–Mar 2012	Daily mean	23	Lawson et al. (2015)
Tropical Eastern Pacific Ocean	15°S–5°N	85°W–95°W	Nov 2008–Jan 2009	Daily mean	67	Sinreich et al. (2010)
Cape Verde	17°N	25°W	Jun–Sep 2014	Daily mean	5.6	Walker et al. (2022)
North Atlantic	40°N–70°N	10°W–10°E	Sep–Oct 2017	Daily mean	19	Kluge et al. (2023), 0–2 km mean
Tropical Atlantic	6°S–35°N	40°W–3°E	Aug 2018	Daily mean	44	Kluge et al. (2023), 0–2 km mean
East China Sea	17°N–33°N	122°E–135°E	Mar 2018	Daily mean	75	Kluge et al. (2023), 0–2 km mean
Weddell Sea	43°S–60°S	34°W–75°W	Oct 2019	Daily mean	10	Kluge et al. (2023), 0–2 km mean
Land						
Amazon	12°S–2°N	51°W–68°W	Sep 2014	Daily mean	87	Kluge et al. (2020), 0–2 km mean
Hong Kong	22.217°N	114.25°E	Nov 2020–Feb 2021	10–15 Local time	45	Xu et al. (2023)
Xingtai	37.18°N	114.37°E	Aug 2021	6–18 Local time	80	Wang et al. (2019)
Shenzhen	22.55°N	114.60°E	Sep–Oct 2019	Daily mean	289	Zhu et al. (2021)
Guangzhou	23°N	113.2°E	Sep–Nov 2018	Daily mean	1	Wu et al. (2020)
Hua Guo Shan	22.728°N	112.929°E	Jan 2017	Daily mean	100	Chang et al. (2019)
Mt. Hua	34.48°N	110.08°E	Aug 2020	Daily mean	330	Zhang et al. (2024)
Tazhong	38.97°N	83.66°E	May–Jun 2018	Daily mean	210	Geng et al. (2022)
Mt. Hua	34.48°N	110.083°E	Aug 2020	Daily mean	260	Qi et al. (2023)
Shanghai	31.34°N	121.51°E	Jun–Aug 2018	Daily mean	162	Guo et al. (2021)
Mt. Fuji-May	32.81°N	130.73°E	May 2016	Daily mean	30	Mitsuishi et al. (2018)
Mt. Fuji-Dec	32.81°N	130.73°E	Dec 2016	Daily mean	5	Mitsuishi et al. (2018)
Sierra Nevada Mountains	38.88°N	120.62°W	Jul 2009	Daily mean	33	DiGangi et al. (2012)
Mexico City	19.5°N	99°W	Apr 2003	Daily mean	270	Volkamer et al. (2007)

(Continued)

Table S1. Observed surface or boundary layer mean glyoxal concentration over land and ocean. (Continued)

Name	Latitude	Longitude	Period	Hour of Day	Glyoxal (ppt)	Reference
Shanghai	31.19°N	121.43°E	May–Jun 2021	Daily mean	0.6	Chen et al. (2025), below detection limit
Hefei-MAM	31.78°N	117.2°E	Mar 2018–May 2018	8–17 Local time	230	Hong et al. (2022)
Hefei-JJA	31.78°N	117.2°E	Jun 2018–Aug 2018	8–17 Local time	220	Hong et al. (2022)
Hefei-SON	31.78°N	117.2°E	Sep 2018–Nov 2018	8–17 Local time	220	Hong et al. (2022)
Hefei-DJF	31.78°N	117.2°E	Dec 2018–Feb 2019	8–17 Local time	230	Hong et al. (2022)
Elizabeth-MAM	40.66°N	74.21°W	Mar–May, 2000–2001	Daily mean	718	Liu et al. (2006)
Elizabeth-JJA	40.66°N	74.21°W	Jun–Aug, 1999–2000	Daily mean	706	Liu et al. (2006)
Elizabeth-SON	40.66°N	74.21°W	Sep–Nov, 1999–2000	Daily mean	509	Liu et al. (2006)
Elizabeth-DJF	40.66°N	74.21°W	Dec–Feb, 1999–2001	Daily mean	448	Liu et al. (2006)
Lhasa	29.63°N	91.02°E	Aug 2000	Daily mean	400	Li et al. (2022)
Madrid-MAM	40.44°N	3.69°E	Mar 2016–May 2016	9 Local time	1410	Benavent et al. (2019)
Madrid-JJA	40.44°N	3.69°E	Jun 2016–Aug 2016	9 Local time	1040	Benavent et al. (2019)
Madrid-SON	40.44°N	3.69°E	Sep 2016–Nov 2016	9 Local time	980	Benavent et al. (2019)
Madrid-DJF	40.44°N	3.69°E	Dec 2016, Jan–Feb 2016	9 Local time	1400	Benavent et al. (2019)
Chongqing	29.83°N	107.01°E	Dec 2018–Jan 2019	9–16 Local time	80	Xing et al. (2020)
Montelibretti	42.11°N	12.63°E	Jul–Sep 2005	8–16 Local time	440	Possanzini et al. (2007)
Palaiseau-summer	48.71°N	2.21°E	Jul 2009	Daily mean	47	Ait-Helal et al. (2014)
Palaiseau-winter	48.71°N	2.21°E	Jan–Feb 2010	Daily mean	158	Ait-Helal et al. (2014)
Rio de Janeiro-May	22.86°N	43.26°W	May 1999	Daytime	201	Grosjean et al. (2002)
Rio de Janeiro-JJA	22.86°N	43.26°W	Jul–Aug 2000	Daytime	126	Grosjean et al. (2002)
Rio de Janeiro-SON	22.86°N	43.26°W	Sep–Nov 2000	Daytime	99	Grosjean et al. (2002)
Blodgett Forest	38.9°N	120.63°W	Aug–Sep 2000	8–21 Local time	27	Spaulding et al. (2003)
Bukit Atur	4.8°N	117.83°E	Apr–Jul 2008	Daily mean	335	MacDonald et al. (2012)
Mt. Tai	36.25°N	117.1°E	Jun 2006	Daily mean	188	Kawamura et al. (2013)
Tomakomai Forest	42.73°N	141.52°E	Sep 2003	Daily mean	27	Ieda et al. (2006)
Melbourne-MAM	37.69°S	144.95°E	Mar–May, 2017–2019	6–17 Local time	164	Fayad et al. (2020)
Melbourne-JJA	37.69°S	144.95°E	Jun–Aug, 2017–2018	6–17 Local time	139	Fayad et al. (2020)
Melbourne-SON	37.69°S	144.95°E	Sep–Nov, 2017–2018	6–17 Local time	142	Fayad et al. (2020)
Melbourne-DJF	37.69°S	144.95°E	Dec–Feb, 2016–2019	6–17 Local time	134	Fayad et al. (2020)
Beijing	39.9°N	116.41°E	Jun 2017	Daily mean	116	Liang et al. (2013)
Los Angeles	34°N	118°W	Jun 2017	Daily mean	103	Washenfelder et al. (2011)
Manitou Forest	39°N	105°W	May–Jun 2010	Daily mean	28	Wolfe et al. (2014)
Madison	43°N	89°W	Aug 2010	Daily mean	38	Henry et al. (2012)
Alabama	33°N	87°W	May 2011	Daily mean	29	Kaiser et al. (2016)
SOAS	33°N	87°W	Jun–Jul 2013	Daily mean	33	Hettiyadura et al. (2017)
Northern Michigan	45.5°N	84.72°W	Jun–Jul 2013	Daily mean	30	Johnson (2008)
Simcoe	43°N	80°W	Jul 2008	Daily mean	500	Aiello and McLaren (2009)
Wuhan	31°N	114°E	Aug 2021	Daily mean	420	Huang et al. (2023)
Amazon-DJF	2.1°S	59°W	Dec 2019–Feb 2020	Daily mean	70	Donner et al. (2024)
Amazon-MAM	2.1°S	59°W	Mar–May 2020	Daily mean	55	Donner et al. (2024)
Amazon-JJA	2.1°S	59°W	Jun–Aug 2019	Daily mean	69	Donner et al. (2024)

(Continued)

Table S1. Observed surface or boundary layer mean glyoxal concentration over land and ocean. (Continued)

Name	Latitude	Longitude	Period	Hour of Day	Glyoxal (ppt)	Reference
Amazon-SON	2.1°S	59°W	Sep–Nov 2019	Daily mean	80	Donner et al. (2024)

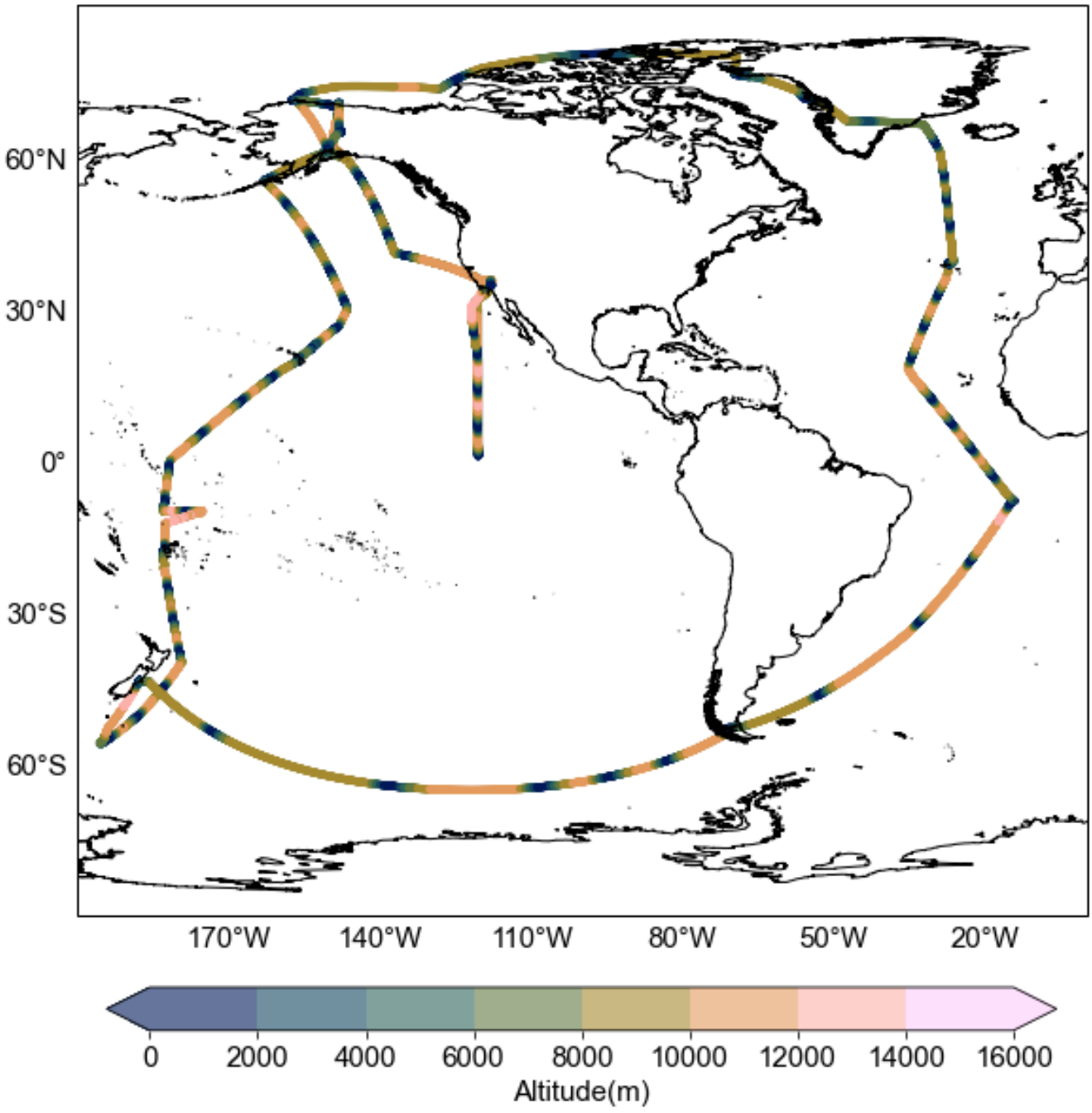

Figure S1. The flight track of the ATom-2 mission.

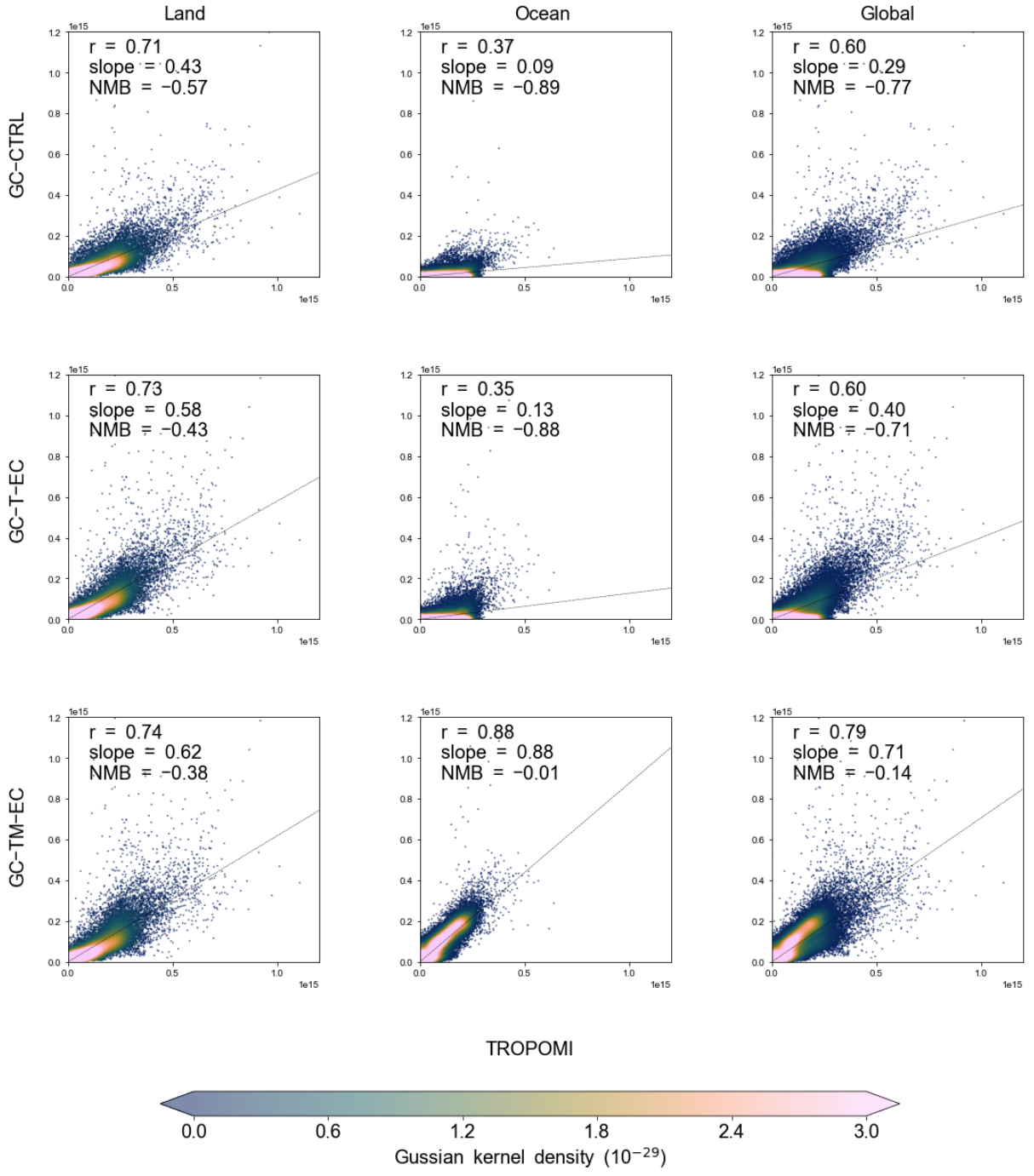

Figure S2. Glyoxal VCDs (molecules cm^{-2}) from TROPOMI observations and GEOS-Chem simulations (GC-CTRL and GC-TM-EC) over land and ocean. Each scatter represents a monthly mean glyoxal VCD over a $2.5^{\circ} \times 2^{\circ}$ grid box.

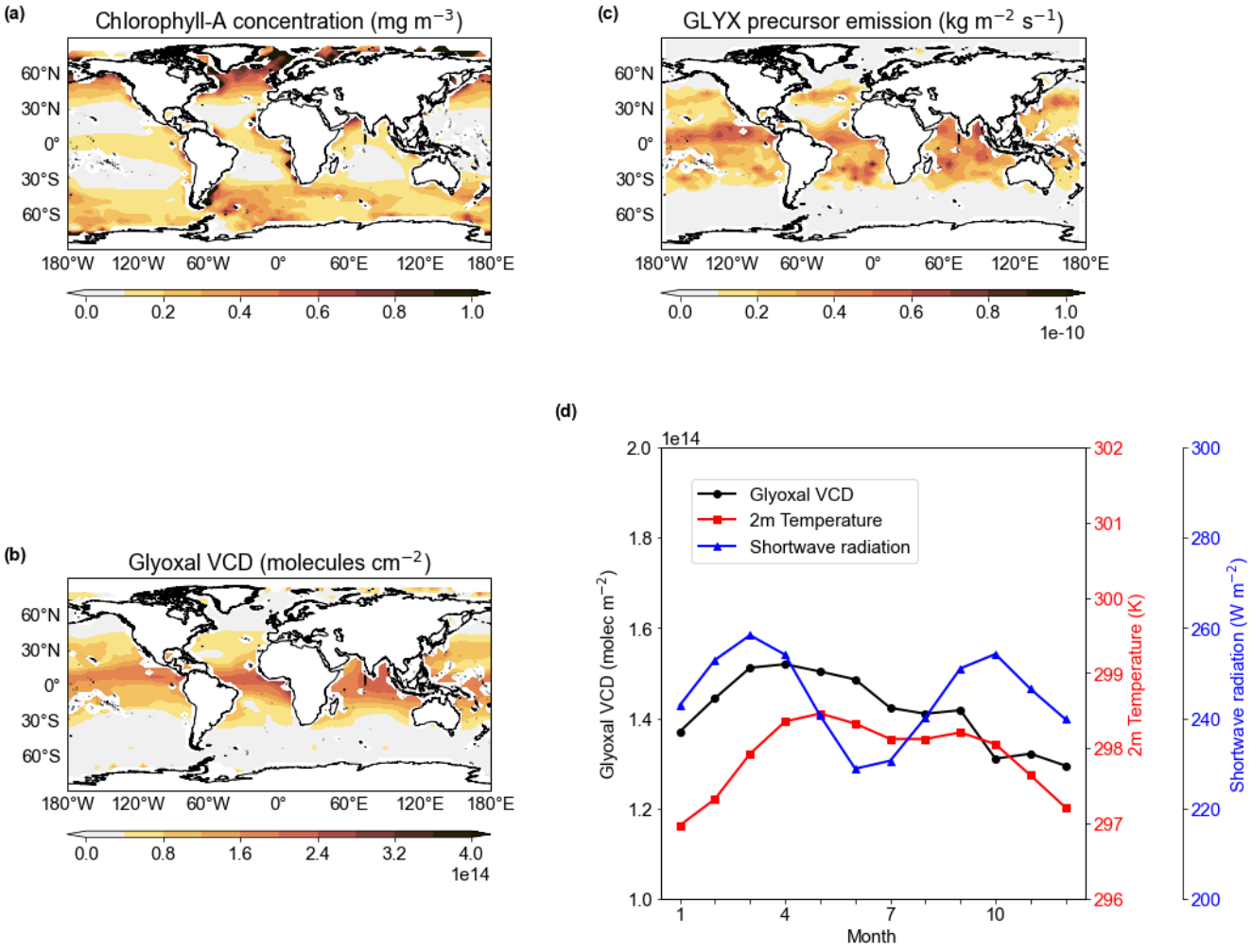

Figure S3. (a) Annual mean chlorophyll-A concentrations in surface sea water retrieved by the MODIS instrument; (b) annual mean TROPOMI-observed glyoxal VCD over the ocean; (c) annual mean emissions of the hypothetical marine precursor of glyoxal as estimated in this study; (d) seasonal variation of TROPOMI-observed glyoxal VCD, 2-m air temperature, and surface downward shortwave radiation flux over the tropical ocean (30° S–30° N).

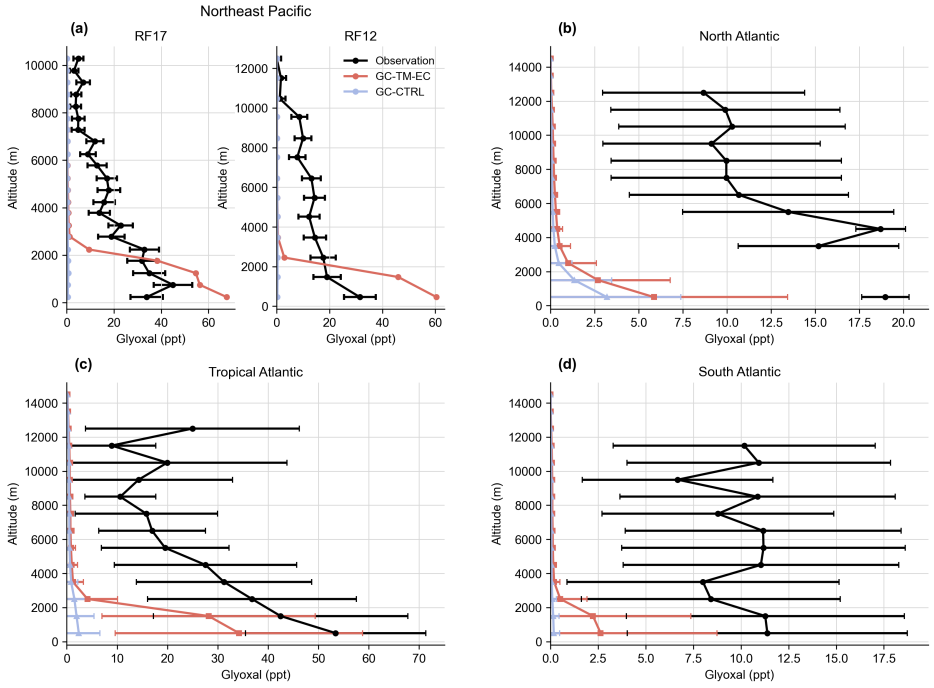

Figure S4. Observed (black) and simulated vertical profiles of glyoxal (a) over the Northeast Pacific during two flights RF17 and RF12 as reported by Volkamer et al. (2015), and over (b) the North Atlantic, (c) the Tropical Atlantic, and (d) the South Atlantic during multiple flights as reported by Kluge et al. (2023). Simulated results from the GC-CTRL (blue) and GC-TM-EC (red) experiments were sampled at the coordinates of the measurements during the month of measurements. Whiskers indicate standard deviations within each vertical layer.

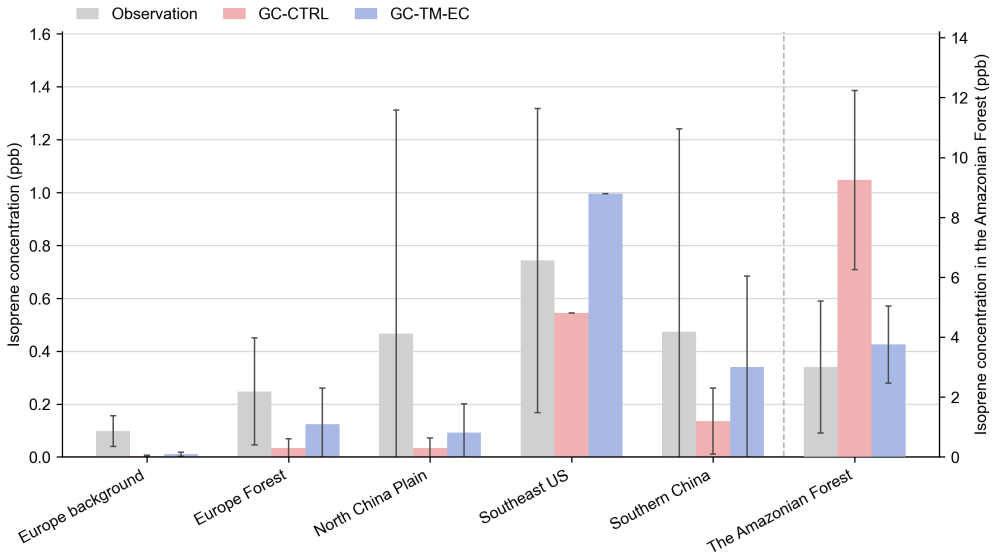

Figure S5. Evaluations of GEOS-Chem simulated surface isoprene concentrations (unit: ppb) against measurements in major source areas of biogenic isoprene: Europe background (Garg et al., 2026), Europe forest (Seco et al., 2011), Amazonian forest (Sun et al., 2025), North China Plain (Zhang et al., 2020), South China (Zhang et al., 2020) and Southeast US forest (Link et al., 2015). The Amazonian forest site is plotted on a separate linear axis because of its much higher concentration range.

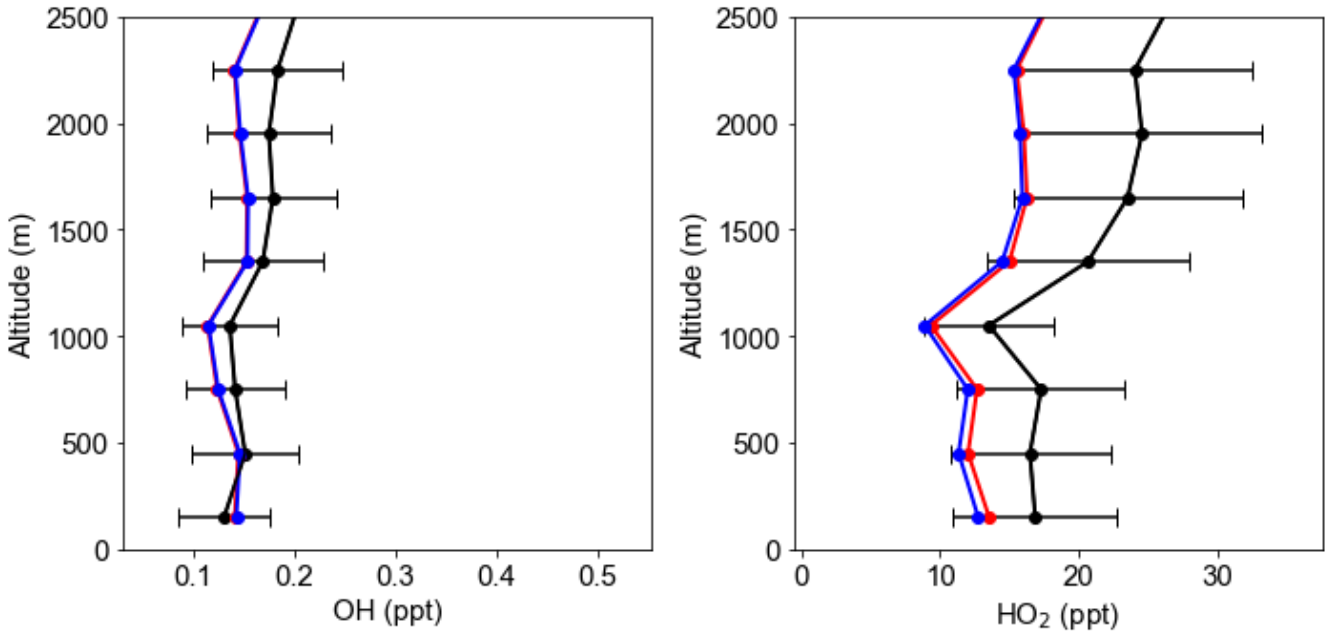

Figure S6. The vertical profiles of ATom-2 aircraft measurements over the tropical ocean (20°S-20°N) and corresponding simulated OH and HO_2 concentrations (GC-CTRL in blue; GC-TM-EC in red) within the MBL.

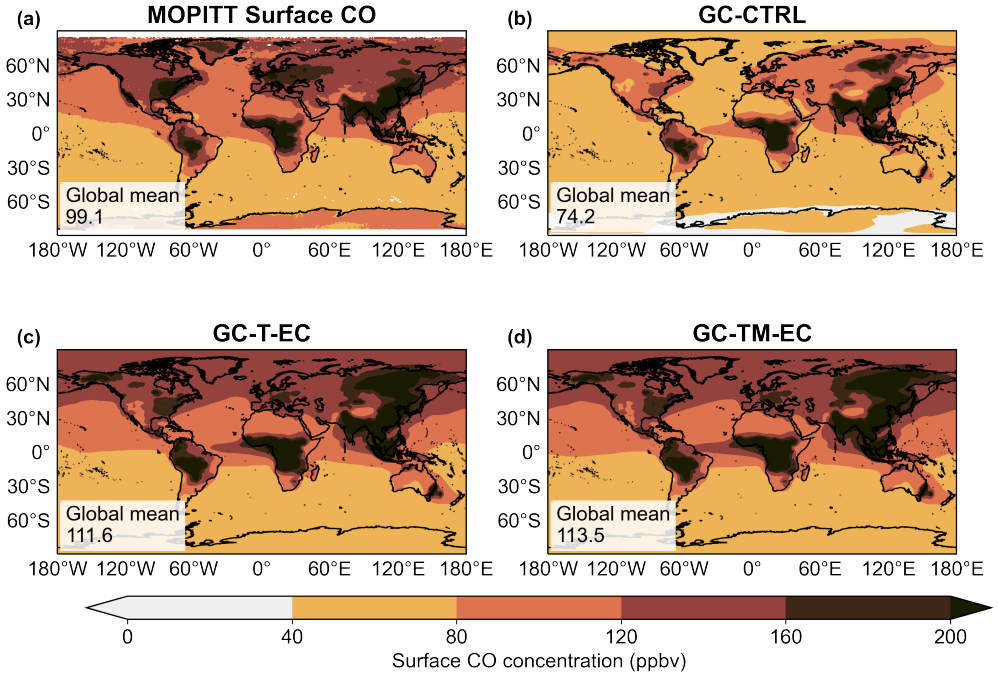

Figure S7. The annual mean (a) MOPITT-retrieved surface CO concentrations and simulated surface CO concentrations in the (b) GC-CTRL, (c) GC-T-EC and (d) GC-TM-EC experiments (unit: ppb) from July 2019 to June 2020. For MOPITT, the annual mean surface CO was derived from the average of the daytime and nighttime retrievals, corresponding to approximately 10:30 and 22:30 local time, respectively.

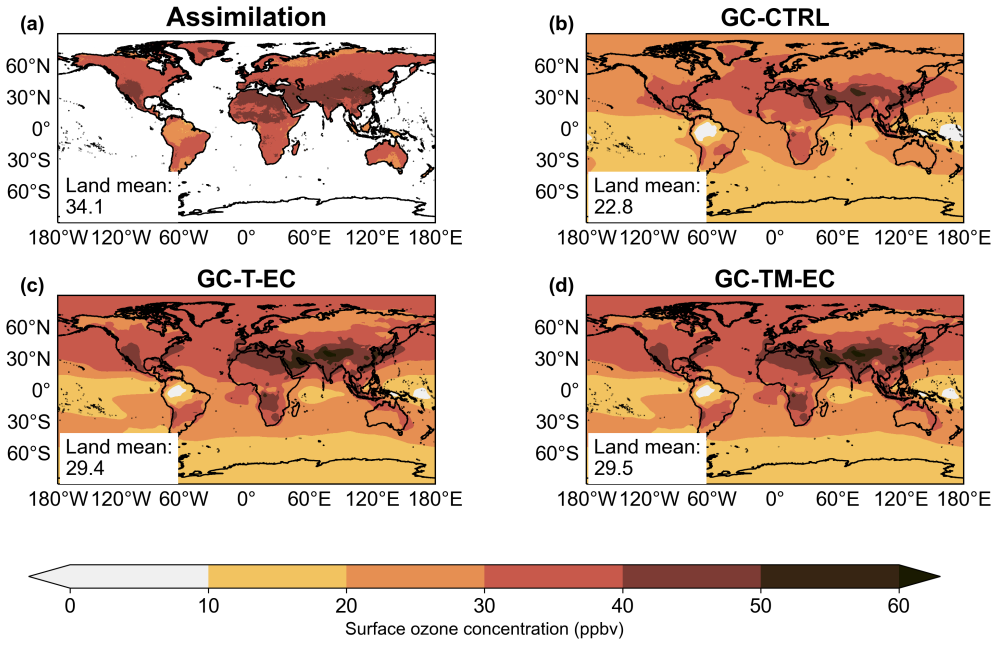

Figure S8. The annual mean (a) assimilated global surface ozone concentrations over land (Wang et al., 2025) and simulated surface ozone concentrations in the (b) GC-CTRL, (c) GC-T-EC and (d) GC-TM-EC experiments (unit: ppb) from July 2019 to June 2020.

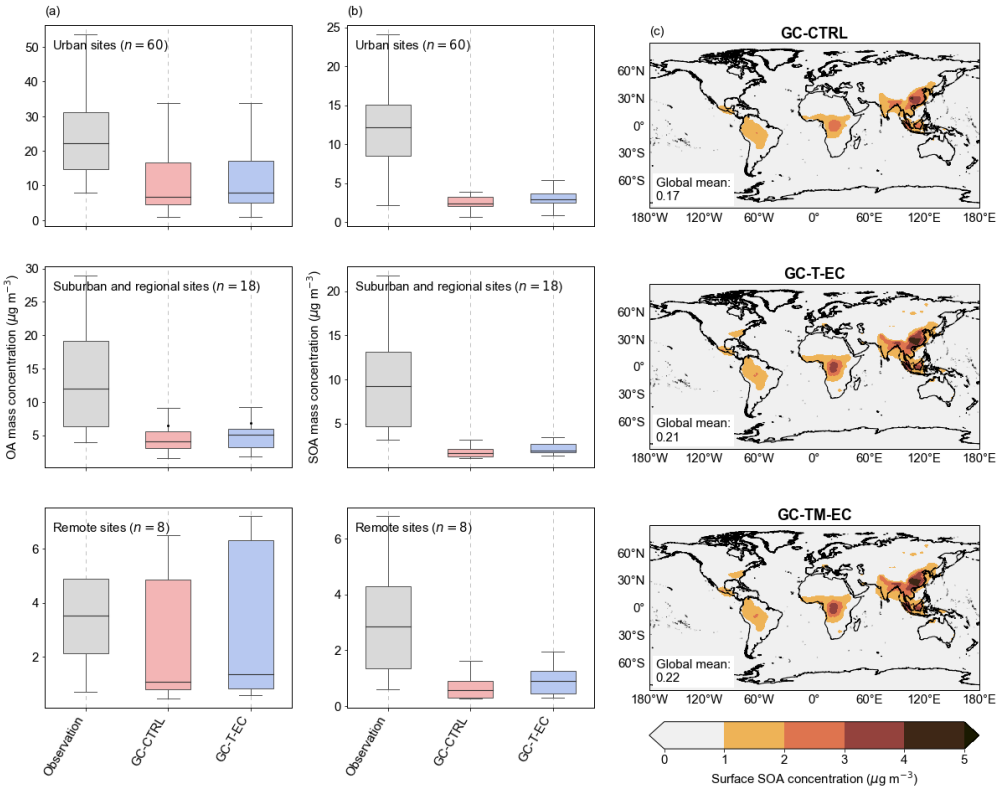

Figure S9. Evaluations of GEOS-Chem simulated (a) OA and (b) SOA against the measurements summarized by Miao et al. (2021) in China. In each boxplot, the horizontal line marks the median, the box represents the interquartile range (25th to 75th percentiles). The whiskers indicate the spread of the corresponding observations and simulations. (c) The simulated annual mean surface SOA concentration in GC-CTRL, GC-T-EC and GC-TM-EC (unit: μg m^{-3}) from July 2019 to June 2020.

References

Aiello, M. and McLaren, R.: Measurement of Airborne Carbonyls Using an Automated Sampling and Analysis System, Environmental Science & Technology, 43, 8901–8907, https://doi.org/10.1021/es901892f, 2009.

Ait-Helal, W., Borbon, A., Sauvage, S., de Gouw, J. A., Colomb, A., Gros, V., Freutel, F., Crippa, M., Afif, C., Baltensperger, U., Beekmann, M., Doussin, J.-F., Durand-Jolibois, R., Fronval, I., Grand, N., Leonardis, T., Lopez, M., Michoud, V., Miet, K., Perrier, S., Prévôt, A. S. H., Schneider, J., Siour, G., Zapf, P., and Locoge, N.: Volatile and intermediate volatility organic compounds in suburban Paris: variability, origin and importance for SOA formation, Atmospheric Chemistry and Physics, 14, 10 439–10 464, https://doi.org/10.5194/acp-14-10439-2014, 2014.

Benavent, N., Garcia-Nieto, D., Wang, S., and Saiz-Lopez, A.: MAX-DOAS measurements and vertical profiles of glyoxal and formaldehyde in Madrid, Spain, Atmospheric Environment, 199, 357–367, https://doi.org/10.1016/j.atmosenv.2018.11.047, 2019.

Chang, D., Wang, Z., Guo, J., Li, T., Liang, Y., Kang, L., Xia, M., Wang, Y., Yu, C., Yun, H., Yue, D., and Wang, T.: Characterization of organic aerosols and their precursors in southern China during a severe haze episode in January 2017, Science of The Total Environment, 691, 101–111, https://doi.org/10.1016/j.scitotenv.2019.07.123, 2019.

Chen, Y., Xu, Y., Huang, D., Lai, D., Chen, Y., Guo, J., Feng, X., Hui, L., Wang, Q., Huang, C., Wang, H., and Wang, Z.: Photochemical impacts of atmospheric carbonyl compounds on ozone formation and radical chemistry in urban Shanghai, Environmental Pollution, 380, 126 557, https://doi.org/10.1016/j.envpol.2025.126557, 2025.

Coburn, S., Ortega, I., Thalman, R., Blomquist, B., Fairall, C. W., and Volkamer, R.: Measurements of diurnal variations and eddy covariance (EC) fluxes of glyoxal in the tropical marine boundary layer: description of the Fast LED-CE-DOAS instrument, Atmospheric Measurement Techniques, 7, 3579–3595, https://doi.org/10.5194/amt-7-3579-2014, 2014.

DiGangi, J. P., Henry, S. B., Kammrath, A., Boyle, E. S., Kaser, L., Schnitzhofer, R., Graus, M., Turnipseed, A., Park, J.-H., Weber, R. J., Hornbrook, R. S., Cantrell, C. A., Maudlin III, R. L., Kim, S., Nakashima, Y., Wolfe, G. M., Kajii, Y., Apel, E., Goldstein, A. H., Guenther, A., Karl, T., Hansel, A., and Keutsch, F. N.: Observations of glyoxal and formaldehyde as metrics for the anthropogenic impact on rural photochemistry, Atmospheric Chemistry and Physics, 12, 9529–9543, https://doi.org/10.5194/acp-12-9529-2012, 2012.

Donner, S., Lauster, B., Ziegler, S., Artaxo, P., Beirle, S., Gurk, C., Lamneck, M., and Wagner, T.: Investigating vertical gradients of trace gases and aerosol at the Amazon Tall Tower Observatory (ATTO) using MAX-DOAS measurements, in: EGU General Assembly Conference Abstracts, p. 7417, 2024.

Fayad, L., Coeur, C., Fagniez, T., Secordel, X., Houzel, N., Mouret, G., Ryan, R. G., Rhodes, S., Tully, M., and Schofield, R.: Surface ozone exceedances in Melbourne, Australia are shown to be under NOx control, as demonstrated using formaldehyde:NO2 and glyoxal:formaldehyde ratios, Science of The Total Environment, 749, 141 460, https://doi.org/10.1016/j.scitotenv.2020.141460, 2020.

Garg, A., Desservettaz, M., Christodoulou, A., Christoudias, T., Kanawade, V. P., Savvides, C., Vrekoussis, M., Naqui, S., Jokinen, T., Byron, J., Williams, J., Mihalopoulos, N., Liakakou, E., Sciare, J., and Bourtsoukidis, E.: Heat and continental transport shape the variability of volatile organic compounds in the Eastern Mediterranean: insights from multi-year observations and regional modeling, Atmospheric Chemistry and Physics, 26, 2597–2622, https://doi.org/10.5194/acp-26-2597-2026, 2026.

Geng, C., Li, S., Yin, B., Gu, C., Liu, Y., Li, L., Li, K., Zhang, Y., Azzi, M., Li, H., Wang, X., Yang, W., and Bai, Z.: Atmospheric Carbonyl Compounds in the Central Taklimakan Desert in Summertime: Ambient Levels, Composition and Sources, Atmosphere, 13, 761, https://doi.org/10.3390/atmos13050761, 2022.

Grosjean, D., Grosjean, E., and Moreira, L. F. R.: Speciated Ambient Carbonyls in Rio de Janeiro, Brazil, Environmental Science & Technology, 36, 1389–1395, https://doi.org/10.1021/es0111232, 2002.

Guo, Y., Wang, S., Zhu, J., Zhang, R., Gao, S., Saiz-Lopez, A., and Zhou, B.: Atmospheric formaldehyde, glyoxal and their relations to ozone pollution under low- and high-NOx regimes in summertime Shanghai, China, Atmospheric Research, 258, 105 635, https://doi.org/10.1016/j.atmosres.2021.105635, 2021.

Henry, S. B., Kammrath, A., and Keutsch, F. N.: Quantification of gas-phase glyoxal and methylglyoxal via the Laser-Induced Phosphorescence of (methyl)GLyOxal Spectrometry (LIPGLOS) Method, Atmospheric Measurement Techniques, 5, 181–192, https://doi.org/10.5194/amt-5-181-2012, 2012.

Hettiyadura, A. P. S., Jayarathne, T., Baumann, K., Goldstein, A. H., de Gouw, J. A., Koss, A., Keutsch, F. N., Skog, K., and Stone, E. A.: Qualitative and quantitative analysis of atmospheric organosulfates in Centreville, Alabama, Atmospheric Chemistry and Physics, 17, 1343–1359, https://doi.org/10.5194/acp-17-1343-2017, 2017.

Hong, Q., Liu, C., Hu, Q., Zhang, Y., Xing, C., Jinping Ou, Tan, W., Liu, H., Huang, X., and Zhenfeng Wu: Vertical distribution and temporal evolution of formaldehyde and glyoxal derived from MAX-DOAS observations: The indicative role of VOC sources, Journal of Environmental Sciences-china, 122, 92–104, https://doi.org/10.1016/j.jes.2021.09.025, 2022.

Huang, H. B., Cheng, H. R., Hu, K., et al.: Characteristics and sources of dicarbonyl compounds during summer photochemical pollution episodes in Wuhan, China Environmental Science, 43, 5114–5122, 2023.

Ieda, T., Kitamor, Y., Mochida, M., Hirata, R., Hirano, T., Inukai, K., Fujinuma, Y., and Kawamura, K.: Diurnal variations and vertical gradients of biogenic volatile and semi-volatile organic compounds at the Tomakomai larch forest station in Japan, Tellus B: Chemical and Physical Meteorology, 58, https://b.tellusjournals.se/articles/10.1111/j.1600-0889.2006.00179.x, 2006.

Johnson, E. D.: Analysis of glyoxal concentrations among a deciduous forest canopy, Working Paper, University of Michigan Biological Station, http://deepblue.lib.umich.edu/handle/2027.42/62026, 2008.

Kaiser, J., Skog, K. M., Baumann, K., Bertman, S. B., Brown, S. B., Brune, W. H., Crounse, J. D., de Gouw, J. A., Edgerton, E. S., Feiner, P. A., Goldstein, A. H., Koss, A., Misztal, P. K., Nguyen, T. B., Olson, K. F., St. Clair, J. M., Teng, A. P., Toma, S., Wennberg, P. O., Wild, R. J., Zhang, L., and Keutsch, F. N.: Speciation of OH reactivity above the canopy of an isoprene-dominated forest, Atmospheric Chemistry and Physics, 16, 9349–9359, https://doi.org/10.5194/acp-16-9349-2016, 2016.

Kluge, F., Hüneke, T., Knecht, M., Matthias Knecht, Lichtenstern, M., Rotermund, M., Schlager, H., Schreiner, B., and Pfeilsticker, K.: Profiling of formaldehyde, glyoxal, methylglyoxal, and CO over the Amazon: normalized excess mixing ratios and related emission factors in biomass burning plumes, Atmospheric Chemistry and Physics, 20, 12 363–12 389, https://doi.org/10.5194/acp-2020-129, 2020.

Kluge, F., Hüneke, T., Lerot, C., Rosanka, S., Rotermund, M. K., Taraborrelli, D., Weyland, B., and Pfeilsticker, K.: Airborne glyoxal measurements in the marine and continental atmosphere: comparison with TROPOMI observations and EMAC simulations, Atmospheric Chemistry and Physics, 23, 1369–1401, https://doi.org/10.5194/acp-23-1369-2023, 2023.

Lawson, S. J., Selleck, P. W., Galbally, I. E., Keywood, M. D., Harvey, M. J., Lerot, C., Helmig, D., and Ristovski, Z.: Seasonal in situ observations of glyoxal and methylglyoxal over the temperate oceans of the Southern Hemisphere, Atmospheric Chemistry and Physics, 15, 223–240, https://doi.org/10.5194/acp-15-223-2015, 2015.

Liang, S., Qin, M., Xie, P., Duan, J., Fang, W., He, Y., Xu, J., Liu, J., Li, X., Tang, K., Meng, F., Ye, K., Liu, J., and Liu, W.: Development of an incoherent broadband cavity-enhanced absorption spectrometer for measurements of ambient glyoxal and NO_2 in a polluted urban environment, Earth System Science Data, 12, 2499–2512, https://doi.org/10.5194/amt-12-2499-2019, 2013.

Lin, H., Long, M. S., Sander, R., Sandu, A., Yantosca, R. M., Estrada, L. A., Shen, L., and Jacob, D. J.: An Adaptive Auto-Reduction Solver for Speeding Up Integration of Chemical Kinetics in Atmospheric Chemistry Models: Implementation and Evaluation in the Kinetic Pre-Processor (KPP) Version 3.0.0, Journal of Advances in Modeling Earth Systems, 15, e2022MS003 293, https://doi.org/10.1029/2022MS003293, 2023.

Link, M., Zhou, Y., Taubman, B., Sherman, J., Morrow, H., Krintz, I., Robertson, L., Cook, R., Stocks, J., West, M., and Sive, B. C.: A characterization of volatile organic compounds and secondary organic aerosol at a mountain site in the Southeastern United States, Journal of Atmospheric Chemistry, 72, 81–104, https://doi.org/10.1007/s10874-015-9305-5, 2015.

Liu, W., Zhang, J. J., Kwon, J., Weisel, C., Turpin, B., Zhang, L., Korn, L., Morandi, M., Stock, T., and Colome, S.: Concentrations and Source Characteristics of Airborne Carbonyl Compounds Measured Outside Urban Residences, Journal of the Air & Waste Management Association, 56, 1196–1204, https://doi.org/10.1080/10473289.2006.10464539, 2006.

MacDonald, S. M., Oetjen, H., Mahajan, A. S., Whalley, L. K., Edwards, P., Heard, D. E., Jones, C. E., and Plane, J. M. C.: DOAS measurements of formaldehyde and glyoxal above a south-east Asian tropical rainforest, Atmospheric Chemistry and Physics, 12, 5949–5962, https://doi.org/10.5194/acp-12-5949-2012, 2012.

Mitsuishi, K., Iwasaki, M., Takeuchi, M., Okochi, H., Kato, S., Ohira, S.-I., and Toda, K.: Diurnal Variations in Partitioning of Atmospheric Glyoxal and Methylglyoxal between Gas and Particles at the Ground Level and in the Free Troposphere, ACS Earth and Space Chemistry, 2, 915–924, https://doi.org/10.1021/acsearthspacechem.8b00037, 2018.

Possanzini, M., Tagliacozzo, G., and Cecinato, A.: Ambient Levels and Sources of Lower Carbonyls at Montelibretti, Rome (Italy), Water, Air, and Soil Pollution, 183, 447–454, https://doi.org/10.1007/s11270-007-9393-1, 2007.

Qi, W., Zhang, Y., Shen, M., Li, L., Dai, W., Chen, Y., Liu, Y., Guo, X., Cao, Y., Wang, X., Jiang, Y., and Li, J.: Comparison of gas–particle partitioning of glyoxal and methylglyoxal in the summertime atmosphere at the foot and top of Mount Hua, Molecules, 28, 5276, https://doi.org/10.3390/molecules28135276, 2023.

Sandu, A. and Sander, R.: Simulating chemical systems in Fortran90 and Matlab with the Kinetic PreProcessor KPP-2.1, Atmospheric Chemistry and Physics, 6, 187–195, https://doi.org/10.5194/acp-6-187-2006, 2006.

Seaman, V. Y., Charles, M. J., and Cahill, T. M.: A sensitive method for the quantification of acrolein and other volatile carbonyls in ambient air, Analytical Chemistry, 78, 2405–2412, https://doi.org/10.1021/ac051947s, 2006.

Seco, R., Peñuelas, J., Filella, I., Llusià, J., Molowny-Horas, R., Schallhart, S., Metzger, A., Müller, M., and Hansel, A.: Contrasting winter and summer VOC mixing ratios at a forest site in the Western Mediterranean Basin: the effect of local biogenic emissions, Atmospheric Chemistry and Physics, 11, 13 161–13 179, https://doi.org/10.5194/acp-11-13161-2011, 2011.

Sinreich, R., Coburn, S., Dix, B., and Volkamer, R.: Ship-based detection of glyoxal over the remote tropical Pacific Ocean, Atmospheric Chemistry and Physics, 10, 11 359–11 371, https://doi.org/10.5194/acp-10-11359-2010, 2010.

Spaulding, R. S., Schade, G. W., Goldstein, A. H., and Charles, M. J.: Characterization of secondary atmospheric photooxidation products: Evidence for biogenic and anthropogenic sources, Journal of Geophysical Research: Atmospheres, 108, https://doi.org/10.1029/2002JD002478, 2003.

Sun, S., Palmer, P. I., Siddans, R., Kerridge, B. J., Ventress, L., Edtbauer, A., Ringsdorf, A., Pfannerstill, E. Y., and Williams, J.: Seasonal isoprene emission estimates over tropical South America inferred from satellite observations of isoprene, Atmospheric Chemistry and Physics, 25, 15 801–15 818, https://doi.org/10.5194/acp-25-15801-2025, 2025.

Volkamer, R., San Martini, F., Molina, L. T., Salcedo, D., Jimenez, J. L., and Molina, M. J.: A missing sink for gas-phase glyoxal in Mexico City: Formation of secondary organic aerosol, Geophysical Research Letters, 34, https://doi.org/10.1029/2007GL030752, 2007.

Volkamer, R., Baidar, S., Campos, T. L., Coburn, S., DiGangi, J. P., Dix, B., Eloranta, E. W., Koenig, T. K., Morley, B., Ortega, I., Pierce, B. R., Reeves, M., Sinreich, R., Wang, S., Zondlo, M. A., and Romashkin, P. A.: Aircraft measurements of BrO, IO, glyoxal, NO_2, H_2O, O_2–O_2 and aerosol extinction profiles in the tropics: comparison with aircraft-/ship-based in situ and lidar measurements, Atmospheric Measurement Techniques, 8, 2121–2148, https://doi.org/10.5194/amt-8-2121-2015, 2015.

Wang, R., Shen, H., Zeng, C., Chen, J., Wang, Y., and Li, Y.: A global land daily 10-km-resolution surface ozone dataset from 2013–2022, Scientific Data, 12, 1710, https://doi.org/10.1038/s41597-025-05990-x, 2025.

Wang, Y., Dörner, S., Donner, S., Böhnke, S., De Smedt, I., Dickerson, R. R., Dong, Z., He, H., Li, Z., Li, Z., Li, D., Liu, D., Ren, X., Theys, N., Wang, Y., Wang, Y., Wang, Z., Xu, H., Xu, J., and Wagner, T.: Vertical profiles of NO_2, SO_2, HONO, HCHO, CHOCHO and aerosols derived from MAX-DOAS measurements at a rural site in the central western North China Plain and their relation to emission sources and effects of regional transport, Atmospheric Chemistry and Physics, 19, 5417–5449, https://doi.org/10.5194/acp-19-5417-2019, 2019.

Washenfelder, R. A., Young, C. J., Brown, S. S., Angevine, W. M., Atlas, E., Blake, D. R., Bon, D. M., Cubison, M. J., de Gouw, J. A., de Gouw, J. A., de Gouw, J. A., Dusanter, S., Flynn, J., Gilman, J. B., Graus, M., Griffith, S. M., Griffith, S. M., Grossberg, N., Hayes, P. L., Jimenez, J. L., Kuster, W. C., Lefer, B., Pollack, I. B., Ryerson, T. B., Ryerson, T. B., Stark, H., Stevens, P. S., and Trainer, M.: The glyoxal budget and its contribution to organic aerosol for Los Angeles, California, during CalNex 2010, Journal of Geophysical Research, 116, https://doi.org/10.1029/2011jd016314, 2011.

Wolfe, G. M., Cantrell, C., Kim, S., Mauldin III, R. L., Karl, T., Harley, P., Turnipseed, A., Zheng, W., Flocke, F., Apel, E. C., Hornbrook, R. S., Hall, S. R., Ullmann, K., Henry, S. B., DiGangi, J. P., Boyle, E. S., Kaser, L., Schnitzhofer, R., Hansel, A., Graus, M., Nakashima, Y., Kajii, Y., Guenther, A., and Keutsch, F. N.: Missing peroxy radical sources within a summertime ponderosa pine forest, Atmospheric Chemistry and Physics, 14, 4715–4732, https://doi.org/10.5194/acp-14-4715-2014, 2014.

Wu, C., Wang, C., Wang, S., Wang, W., Yuan, B., Qi, J., Wang, B., Wang, H., Wang, C., Song, W., Wang, X., Hu, W., Lou, S., Ye, C., Peng, Y., Wang, Z., Huangfu, Y., Xie, Y., Zhu, M., Zheng, J., Wang, X., Jiang, B., Zhang, Z., and Shao, M.: Measurement report: Important contributions of oxygenated compounds to emissions and chemistry of volatile organic compounds in urban air, Atmospheric Chemistry and Physics, 20, 14 769–14 785, https://doi.org/10.5194/acp-20-14769-2020, 2020.

Xing, C., Liu, C., Hu, Q., Fu, Q., Lin, H., Wang, S., Su, W., Wang, W., Javed, Z., and Liu, J.: Identifying the wintertime sources of volatile organic compounds (VOCs) from MAX-DOAS measured formaldehyde and glyoxal in Chongqing, southwest China, Science of The Total Environment, 715, 136 258, https://doi.org/10.1016/j.scitotenv.2019.136258, 2020.

Xiong, E., Guo, H., Fu, T.-M., Lyu, X., Wang, Y., Zhou, B., Xia, M., Zou, Z., Yuan, Q., Yang, J., Shek, K. Y., Chen, J., Jiang, T., Tao, W., Zhang, A., Xiang, W., Lee, S., and Wang, T.: Complex impacts of oxygenated volatile organic compounds on radical photochemistry in the background air of Southern China, Submitted, 2025.

Xu, Y., Feng, X., Chen, Y., Zheng, P., Hui, L., Chen, Y., Yu, J. Z., and Wang, Z.: Development of an enhanced method for atmospheric carbonyls and characterizing their roles in photochemistry in subtropical Hong Kong, Science of The Total Environment, 896, 165 135, https://doi.org/10.1016/j.scitotenv.2023.165135, 2023.

Zhang, Y., Zhang, R., Yu, J., Zhang, Z., Yang, W., Zhang, H., Lyu, S., Wang, Y., Dai, W., Wang, Y., and Wang, X.: Isoprene Mixing Ratios Measured at Twenty Sites in China During 2012–2014: Comparison With Model Simulation, Journal of Geophysical Research: Atmospheres, 125, e2020JD033 523, https://doi.org/10.1029/2020JD033523, 2020.

Zhang, Y., Dai, W., Li, J., Ho, S. S. H., Li, L., Shen, M., Wang, Q., and Cao, J.: Comprehensive observations of carbonyls of Mt. Hua in Central China: Vertical distribution and effects on ozone formation, Science of The Total Environment, 907, 167 983, https://doi.org/10.1016/j.scitotenv.2023.167983, 2024.

Zhou, X. and Mopper, K.: Apparent partition coefficients of 15 carbonyl compounds between air and seawater and between air and freshwater; implications for air-sea exchange, Environmental Science & Technology, 24, 1864–1869, https://doi.org/10.1021/es00082a013, 1990.

Zhu, B., Huang, X.-F., Xia, S.-Y., Lin, L.-L., Cheng, Y., and He, L.-Y.: Biomass-burning emissions could significantly enhance the atmospheric oxidizing capacity in continental air pollution, Environmental Pollution, 285, 117 523, https://doi.org/10.1016/j.envpol.2021.117523, 2021.

Zou, Z., Chen, Q., Xia, M., Yuan, Q., Chen, Y., Wang, Y., Xiong, E., Wang, Z., and Wang, T.: OH measurements in the coastal atmosphere of South China: possible missing OH sinks in aged air masses, Atmospheric Chemistry and Physics, 23, 7057–7074, https://doi.org/10.5194/acp-23-7057-2023, 2023.